10th International Conference on Fracture Mechanics of Concrete and Concrete Structures
FraMCoS-X
G. Pijaudier-Cabot, P. Grassl and C. La Borderie (Eds)
https://doi.org/10.21012/FC10.235632

COLLAPSE SIMULATION OF REINFORCED CONCRETE INCLUDING LOCALIZED FAILURE AND LARGE ROTATION USING EXTENDED RBSM

YOSHIHITO YAMAMOTO*, YU ISAJI†, HIKARU NAKAMURA* AND TAITO MIURA*

* Nagoya University
Furo-cho, Chikusa-ku, Nagoya, 464-8603, Japan
e-mail: y.yamamoto@civil.nagoya-u.ac.jp, www.nagoya-u.ac.jp

† Obayashi Corporation
Shinagawa Intercity Tower B, 2-15-2, Konan, Minato-ku, Tokyo 108-8502, Japan
e-mail: isaji.yu@obayashi.co.jp, www.obayashi.co.jp

Key words: Damage localization, Post-peak behavior, Geometric nonlinearity, Finite rotation, Rigid-Body-Spring Model, Timoshenko beam element

Abstract: In this study, an extended Rigid-Body-Spring Model (RBSM) considering geometric nonlinearity including finite rotation is developed based on an equivalence between the RBSM and the reduced integration Timoshenko beam element in order to simulate not only damage localization behavior but also large displacement and large rotation collapse behavior of reinforced concrete structures. Firstly, an elastic buckling response of a column is simulated by using the proposed method. By comparing the simulation result and the exact solution, it is confirmed that the proposed model can reproduce the large displacement and large rotation behavior in the elastic range. In addition, several numerical simulations of failure behavior of concrete and reinforced concrete members are presented. It is also confirmed that the model can simulate localized damage, rebar buckling and large rotational collapse behavior.

1 INTRODUCTION

A numerical simulation model that can accurately reproduce not only post-peak behavior of concrete members including damage localization, rebar buckling and so on but also collapse behavior of entire concrete structures will be an effective tool for assessing the restorability and redundancy of infrastructure systems subjected to extreme loads exceeding design requirements such as earthquakes, impact loads and so on.

In order to accurately reproduce post-peak behavior of reinforced concrete members, it is necessary to reproduce softening and damage localization behavior of concrete under various stresses, especially under compression including lateral confinement effect. However, it is difficult to reproduce the damage localization behavior by numerical simulation methods based on continuum mechanics such as a finite element method. In order to overcome them, many researches have been conducted, for example, on the application of nonlocal constitutive models and so on [1-3].

On the other hands, many lattice and particle type discretization models have been proposed for reproducing fracture and failure behvaior on concrete, concrete structures or other quasi-brittle material [4-9]. By applying a random network model with Voronoi tessellation and by introducing non-linear constitutive models of the combination of normal and shear components between nodes or particles, and so on, these models have become possible to reproduce the above-mentioned localization behavior [9].

A Rigid-Body-Spring Model (RBSM) proposed by Kawai [10] is a discrete type numerical simulation method which is similar to the above-mentioned lattice and particle type models. Bolander and Saito [11] have introduced a random geometry to the RBSM mesh using Voronoi tessellation and simple reinforcing steel bar model considering the nonlinear bond characteristics between concrete and rebar by beam and link elements, and they have also demonstrated that the model can simulate the crack patterns, the deformation and the load capacity of concrete materials and reinforced concrete structures. Nagai et al. [12] have developed a three-dimensional RBSM and applied to simulations of softening and damage localization behavior on concrete material. They have shown that the model can represent the multi-axial compression behaviour including softening and damage localization with the simple constitutive models. The authors have also developed the three-dimensional RBSM and constitutive models to quantitatively evaluate mechanical response of concrete including strain softening and damage localization behavior under various stress conditions [13,14], and have also demonstrated that the model can well simulate cracking and damage localization behavior in concrete and reinforced concrete structures [15-18]. However, since the existing lattice and particle type discretization models including the RBSM do not consider a geometric nonlinearity, they cannot reproduce collapse behavior including large displacement and large rotation which occur after softening and damage localization of concrete.

In this study, an extended RBSM considering geometric nonlinearity including finite rotation is developed in order to simulate not only softening and damage localization but also large displacement and large rotation collapse behavior of reinforced concrete structures. In addition, through simulations of an elastic column, a plain concrete and a reinforced concrete beam, validity and usefulness of the proposed method are demonstrated.

2 NUMERICAL MODELING

In this chapter, at first, basic concepts, constitutive models, modeling of reinforcing steel bar of the existing RBSM proposed by the authors [13,14,17], which is the basis of the extension model proposed in this study, are briefly described. Then, an extended RBSM considering geometric non-linearity including finite rotation is described.

2.1 RBSM

In the RBSM, a total of 6 degrees of freedom, 3 for translation and 3 for rotation, are set at representative points in the element as shown in Fig. 1, and a rigid-body motion is assumed for each element. Note that a rotation matrix based on the assumption of infinitesimal rotation is generally used for the description of a rigid-body motion of the elements. Springs consisting of one normal and two shear components are set at an arbitrary point on the interface between two rigid elements. Strains of the springs are evaluated from the relative displacement in a local coordinate system defined by the normal and tangential directions to the interface between two elements, and stresses of the springs are evaluated by non-linear constitutive models shown in 2.2. In particular, the strains of the springs are assumed by the following formula.

$$\varepsilon = \delta_n / h \tag{1a}$$

$$\gamma_l = \delta_l / h \tag{1b}$$

$$\gamma_m = \delta_m / h \tag{1c}$$

where, ε, γ_l and γ_m are the strains of the normal and two shear springs, respectively. In addition, δ_n, δ_l and δ_m are relative displacements at the evaluation points between the two elements in the local coordinate system. h is a sum of distances from the centroid (or Voronoi generator point) of the two elements to the boundary Voronoi face. By applying the strain and the displacement relationship and the constitutive models to the incremental linearized virtual work equation, an incremental linearized system equilibrium

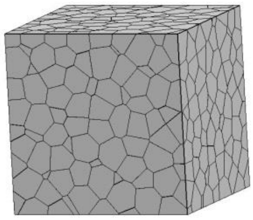

(a) Domain discretization using Voronoi diagram

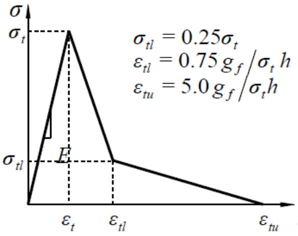

(a) Tensile model of the normal spring

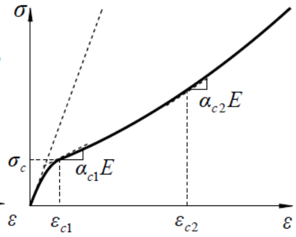

(b) Compression model of the normal spring

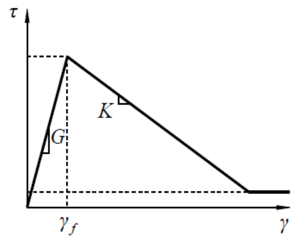

(c) Response of resultant shear stress and strain

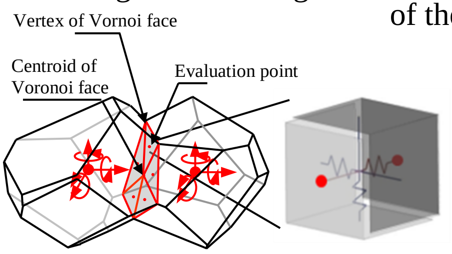

(b) Two-element assembly and springs configuration

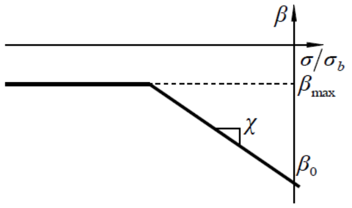

(d) Shear softening coefficient

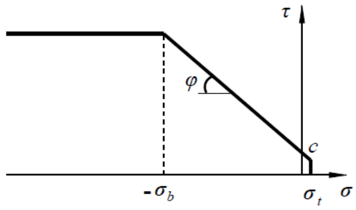

(e) Mohr Coulomb type criterion

Figure 1: Element configuration of the RBSM

Figure 2: Constitutive model for concrete [13,17]

equation is obtained. In this study, the modified Newton-Raphson method is used for unbalanced force minimization.

In this model, a target domain is discretized by a random geometry mesh using Voronoi diagram as shown in Fig. 1. In addition, it is noteworthy that typical RBSM or another particle type models have only one evaluation point (in other words one integration point) in each two elements assembly, whereas the proposed model has multiple evaluation points [13,17]. Specifically, as shown in Fig. 1, the evaluation points are arranged at the centroid of the triangle formed of the centroid and the vertices of the Voronoi face. With this arrangement, the moment resistance between two elements is automatically represented without rotational springs.

2.2 Proposed constitutive models of springs for concrete material [13,17]

The constitutive models for the normal and shear springs are shown in Fig. 2. The tensile model for the normal spring is shown in Fig. 2a. σ_t and g_f are tensile strength and tensile fracture energy. Fig. 2b shows the compression model of the normal springs. A reversed S-shape curve is assumed. For the shear springs, resultant shear stress and resultant shear strain are used. The resultant shear strain is defined by Eq. (2).

$$\gamma = \sqrt{\gamma_l^{\ 2} + \gamma_m^{\ 2}} \tag{2}$$

Then, resultant shear stress τ is calculated from the shear stress–strain relation, and the shear stresses for each direction (τ_l and τ_m) are distributed by Eq. (3).

$$\tau_l = \tau\frac{\gamma_l}{\gamma},\ \ \tau_m = \tau\frac{\gamma_m}{\gamma} \tag{3}$$

The envelope of the resultant shear stress–strain relationship is given in Fig. 2c, Eq. (4) and Eq. (5).

$$\tau = \begin{cases} G\gamma & (\gamma < \tau_{f,soft}/G) \\ \tau_{f,soft} & (\gamma \geq \tau_{f,soft}/G) \end{cases} \tag{4}$$

$$\tau_{f,soft} = \max\left(\tau_f + K\langle\gamma_{\max} - \gamma_f\rangle,\ 0.1\tau_f\right) \tag{5a}$$

$$K = \beta G \tag{5b}$$

$$\beta = \min\left(\beta_0 + \chi(\sigma/\sigma_b),\ \beta_{\max}\right) \tag{5c}$$

where, τ_f, γ_f and $\gamma_{\max}$ are shear strength, strain corresponding to strength and the maximum value of γ in loading history, respectively. The brackets $\langle \cdot \rangle$ in Eq. 5a is defined as $\langle x \rangle = \max(x, 0)$. The resultant shear stress elastically increases up to the shear strength with the slope of the shear modulus G and softening behavior is also assumed. K is the shear softening coefficient that is defined by Eq. (5). It is assumed that the shear softening coefficient K depends upon the stress of the normal spring as represented in Eq. (5) and Fig. 2d, where, β_0, $\beta_{\max}$ and χ are parameters that control a function that represents the normal spring stress dependency of the shear softening coefficient.

The Mohr–Coulomb criterion is assumed as the failure criteria for the shear spring (Fig. 2e and Eq. (6)), where c and φ are cohesion and the angle of internal friction, respectively. The shear strength is assumed to be constant when the normal stress is greater than σ_b, which is termed the compression limit value.

$$\tau_f = \begin{cases} c - \sigma \tan\varphi & (\sigma > -\sigma_b) \\ c + \sigma_b \tan\varphi & (\sigma \leq -\sigma_b) \end{cases} \tag{6}$$

Moreover, it is assumed that the shear stress decreases with an increase in crack width at the cracked surface, in which tensile softening occurs in a normal spring by taking into consideration the shear deterioration coefficient β_{cr} as represented in Eq. (7). Here, ε_t and ε_{tu} are cracking strain and ultimate strain in a normal spring, respectively.

$$\beta_{cr} = \frac{\varepsilon_t}{\varepsilon} \exp\left\{ \frac{\kappa}{\varepsilon_{tu}} \left(\varepsilon - \varepsilon_t \right) \right\} \tag{7}$$

The stiffness on the unloading path for the normal and shear springs are equal to the initial elastic modulus E and G. In addition, after the stress reaches zero on the unloading path, the stress keeps zero until the strain reaches the residual strain of the opposite sign.

The material parameters of the constitutive models as described above has been calibrated by conducting parametric analyses comparing with the test results of uniaxial tension, uniaxial compression, hydrostatic compression and triaxial compression. The parametric analyses include a variety of specimen size, shape, a Voronoi cell size (mesh size) and concrete strengths. The calibrated parameters are shown in Table 1. These parameters are recommended for normal strength concrete. For the simplification, the material parameters are assumed to be uniformly distributed over a discretized concrete area. In practical

Table 1: Model parameters [13]

Normal spring							Shear spring							
Elastic modulus	Tensile response		Compressive response				Elastic modulus	Fracture criterion			Softening behavior			
E N/mm^2	σ_t N/mm^2	g_f N/mm^2	σ_c N/mm^2	ε_{c2}	α_{c1}	α_{c2}	$\eta = G/E$	c N/mm^2	φ degree	σ_b N/mm^2	β_0	β_{max}	χ	κ
1.4E*	0.8f_t*	0.5G_f*	1.5f_c'*	-0.015	0.15	0.25	0.35	0.14f_c'*	37	f_c'*	-0.05	-0.02	-0.01	-0.3

* The macroscopic material parameters obtained from the concrete specimens tests

E* : Young's modulus, f_t* : Tensile strength, G_f* : Fracture energy, f_c'* : Compressive strength

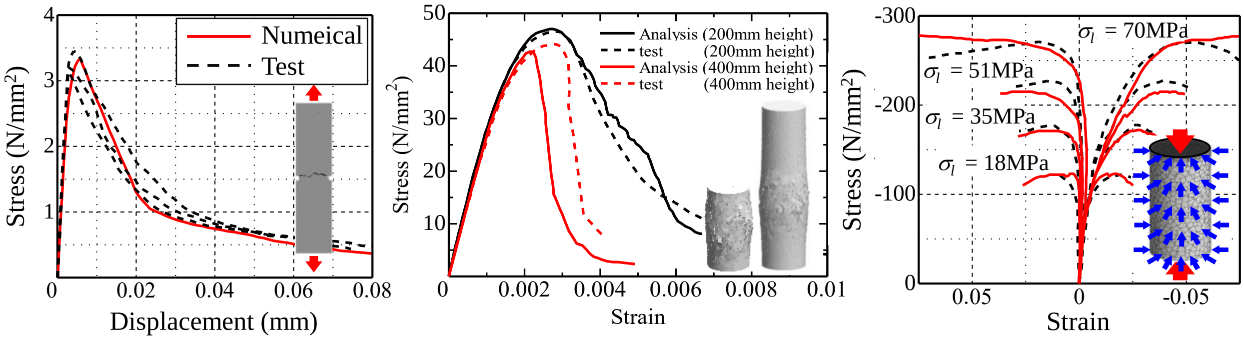

(a) Uniaxial tension [19] (b) Uniaxial compression [20] (c) Tri-axial compression [21]

Figure 3: Average stress - strain response of the model [13]

application, the mesh size is preferable to be larger for the sake of reducing computational cost. It has been confirmed that the proposed model can reasonably simulate the propagation of visible cracks and especially the localization length of compression failure in concrete in the case of that the average mesh size is from 10 mm to 30 mm [13].

The compression model considers neither softening behavior nor failure of the normal springs. However, compressive failure behavior can be simulated with a confinement effect by means of a combination of the normal spring and shear springs. Fig. 3 show examples of the response obtained by the model. It can be seen from the figures that the proposed model quantitatively reproduces the macroscopic softening, damage localization and volume change behavior including confinement pressure dependency. Although not shown here, the proposed model can also quantitatively reproduce the length of the localized damage zone under uniaxial compression [13].

2.3 Modeling of reinforcing steel bar

A reinforcing steel bar is modeled as a series of regular beam elements (Fig. 4a) that can be freely located within the structure, regardless of the concrete mesh design [11]. Three translational and three rotational degrees of freedom are defined at each beam node. The beam elements are attached to the RBSM elements by means of zero-size link elements that provide a load-transfer mechanism between the beam node and the RBSM elements. The section partition method called the fiber model is applied for the modeling of reinforcing steel bar in order to reproduce the nonlinear mechanical behavior including nonlinear moment-curvature relation. The bilinear kinematic hardening model is applied for the steel material. The hardening coefficient is 1/100. Crack development is strongly affected by the bond interaction between concrete and reinforcement. The bond stress-slip relation is provided in the spring parallel to the reinforcement of link element. Fig. 4b shows the applied nonlinear bond stress – slip relation [17].

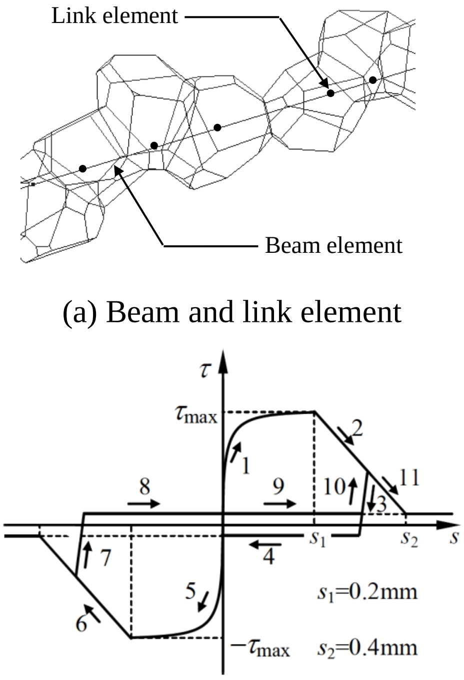

(a) Beam and link element

(b) Bond steress-slip relation

Figure 4: Reinforcing steel bar and bond interface models

2.4 Extension to a model considering geometric nonlinearity

Toi [22] clarified that if the stress and strain evaluation points of the RBSM are arranged on the cross-section of the midpoint between two element nodes, the element stiffness matrix of the RBSM is identical with that of the linear Timoshenko beam element based on the reduced integration technique (one-point quadrature in this case). In this study, we propose the following new model using this equivalence.

Fig. 5 shows an overview of the proposed model. In the model, as shown by the blue line in the figure, the reduced integration Timoshenko beam element considering geometric nonlinearity including finite rotation [23] which has the Voronoi face as a cross-section is applied to the mechanical model between two elements of the RBSM. Here, note that the Voronoi face is always a perpendicular bisector of the line connecting the two Voronoi generator points due to the nature of the Voronoi diagram. That is, by arranging the reduced integration Timoshenko beam element based on Voronoi diagram as

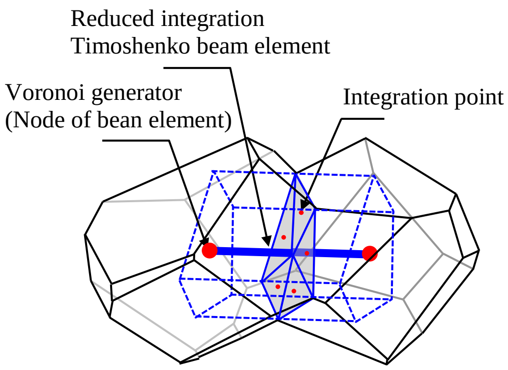

Figure 5: Configuration of reduced integration Timoshenko beam element

shown in Fig. 5, the network structure satisfies the condition of the equivalence proven by Toi [22] described above and therefore is identical with the RBSM in the range of infinitesimal deformation. In other words, the model can reproduce large displacement and large rotation behavior while maintaining the performance of the above-mentioned RBSM.

In the model, the evaluation points (in other words integration points) on the cross-section of the linear Timoshenko beam element are located at the centroid of the triangle consisting of the centroid and vertexes of Voronoi face as in the previous RBSM (Fig. 1). The normal and two shear strain components of Green-Lagrange strain obtained at each integration point are assumed to be the normal and shear strains of the springs. For the calculation of the stress, the same constitutive models as the above-mentioned RBSM proposed by the authors are assumed.

Similarly, the reduced integration Timoshenko beam elements with finite rotation are applied to modeling of reinforcing steel bars. The section partition method and the bilinear kinematic hardening model are also applied.

3 NUMERICAL RESULTS

3.1 Post-buckling deformation behavior of Elastic Columns

The proposed model is verified by simulating post-bucking behavior of elastic column subjected to uniaxial compression. Here, we assume that the material is elastic

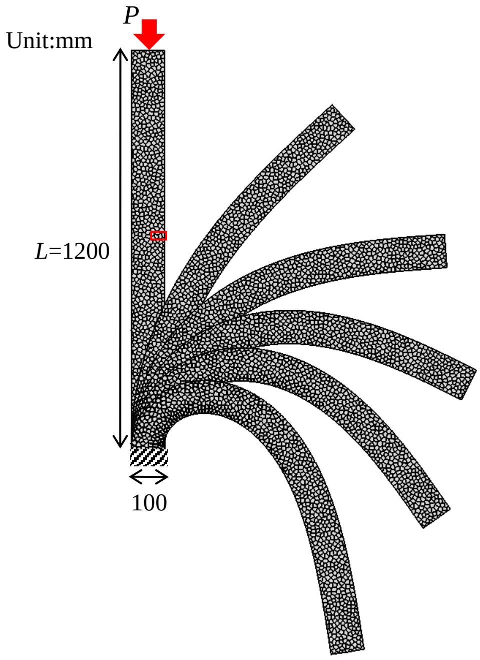

(a) Deformed shape

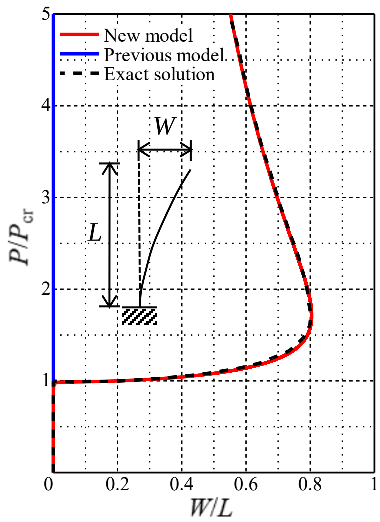

(b) Load – displacement curves

Figure 6: Post-buckling behavior of elastic column

and Poisson's ratio is zero. The elastic modulus of the normal and shear spring is set to equal and the degree of freedom of the RBSM elements (or the nodes of Timoshenko beam element) are locate to the points of Voronoi generator. It should be noted that the RBSM can reproduce elastically homogeneous response of material with Poisson's ratio of 0 when the points of Voronoi generator are selected as the element degrees of freedom of the RBSM and the elastic modulus of the normal and the shear spring is equal [24]. Also, as an initial imperfection, the elastic modulus of the area surrounded by the red line is reduced by 1% from that of the other areas.

The post-buckling deformation behavior and the load and displacement relationship are shown in Fig. 6. An exact solution is also shown in the figures [25]. We can see that the proposed model reproduces the exact solution with high accuracy.

3.2 Collapse behavior of concrete column subjected to eccentric compression

The ability to reproduce large displacement and large rotation behavior is demonstrated by simulating a plain concrete column subjected to eccentric compression. Fig. 7 show collapse behavior obtained by the proposed model. For comparison, simulation results obtained by the existing RBSM are shown in the figures. We can see from the figures that the existing model cannot represent large rotation behavior after penetration of crack. On the other hand, the proposed model can reproduce large rotational behavior until the upper part of the column comes in contact with the lower part in the collapse process. Note that the proposed model cannot reproduce the subsequent contact behavior because it does not update the initial network. We plan to extend the model further in the future.

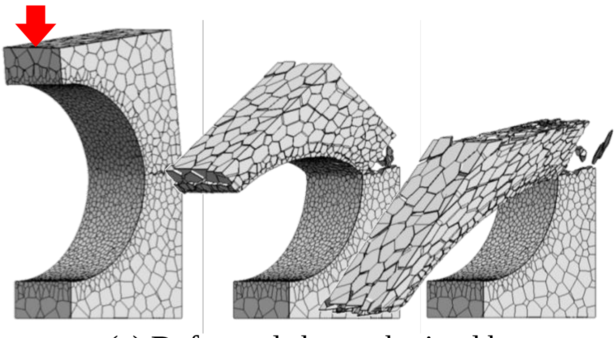

(a) Deformed shape obtained by the existing model

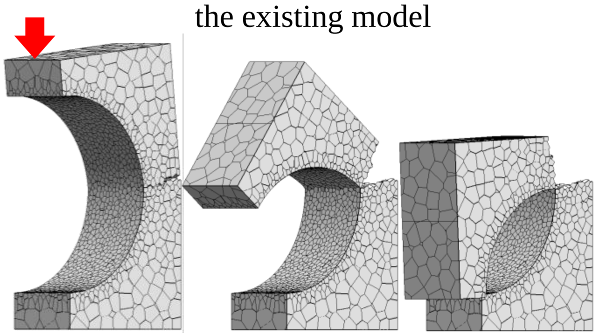

(b) Deformed shape obtained by the proposed model

Figure 7: Collapse behavior after crack penetration of plain concrete

3.3 Post-peak behavior of reinforced concrete beam

In this section, in order to demonstrate the validity and usefulness of the proposed model, simulations of flexural failure type reinforced concrete beam tests are presented. Fig. 8 shows the overview of the test specimen. The compressive strength of concrete is 45.4N/mm^2, and the yield strengths of tensile rebar, compression rebar and stirrup are 401N/mm^2, 398 N/mm^2 and 632 N/mm^2, respectively. Fig. 9 shows the Voronoi mesh configuration of the reinforced concrete beam. The average element size is 10mm in the section where the bending moment is constant. In the shear spans, the element size increases gradually towards the end of the beam, up to 30 mm at the end.

Fig. 10 shows the load-deflection curves and the deformation behavior of the reinforced concrete beam. For comparison, simulation results by using the existing model is shown in

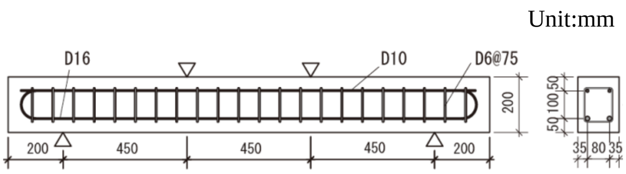

Figure 8: Test specimen

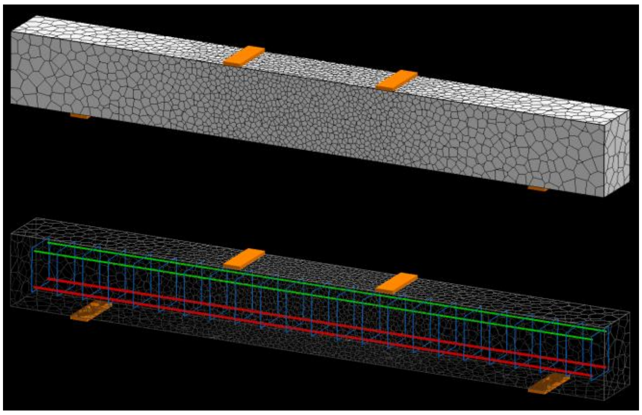

Figure 9: Voronoi mesh configuration of reinforced concrete beam test

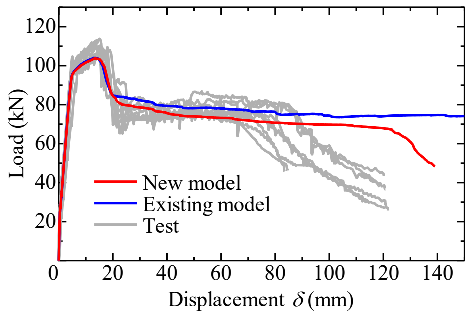

(a) Load – displacement curves

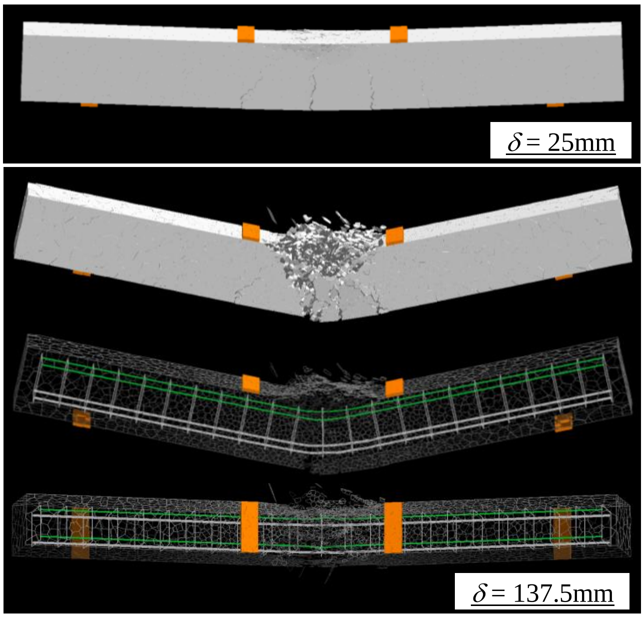

(b) Deformed shape obtained by the existing model

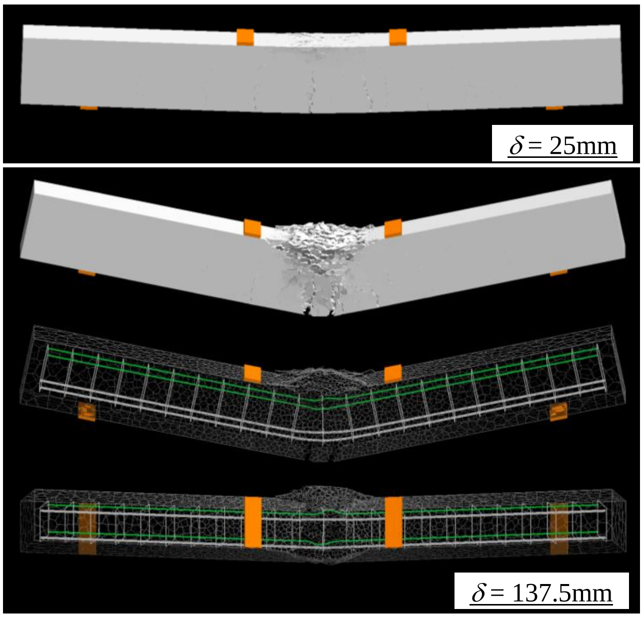

(c) Deformed shape obtained by the proposed model

Figure 10: Post-peak behavior of RC beam

Figure 11: Typical examples of rebar buckling and surrounding concrete failure

the figures. It can be seen from the figures that both models accurately reproduce the maximum load, the maximum load deflection, and the residual load after the first load drop. On the other hand, the existing model does not reproduce the subsequent second load drop. Although the proposed model overestimates the second load drop displacement, it qualitatively reproduces the second load drop. Uncertainty about boundary conditions, such as movement of the loading plates in the test, may be considered as the cause of overestimation, but it is not yet clear and will be investigated in detail in the future.

Fig. 10 also show the deformation behavior just after the first load drop and the second load drop obtained by simulations (in the case of the existing model, the deformation behavior at the same deflection point as the proposed model). It can be seen that, at the time of the first load drop, the compressive failure occurs at the beam upper edge in both simulations results. At the time of the second load drop, in the existing model, unnatural element distortion is observed.

Fig. 11 shows the state of the compression rebar after the test. As shown in the figure, buckling of the compression rebar was observed. Furthermore, compressive failure of core concrete was observed in the area where the rebars were buckled. That is, the decrease in confinement pressure due to the buckling of the rebar caused the second load drop.

Fig. 10 also show the deformation behavior of the compression rebar. Whereas the existing model cannot reproduce the buckling of the rebar, the proposed model can reproduce it.

4 CONCLUSIONS

In this study, an extended RBSM considering geometrical nonlinearity including finite rotation applying the equivalence of RBSM and the reduced integration Timoshenko beam element is proposed. The validity and usefulness of the proposed model are demonstrated through the simulations of post-buckling deformation behavior of elastic column, collapse behavior of plain concrete and post-peak behavior of reinforced concrete beam with flexural failure. The proposed model can reproduce the exact solution of the post-buckling response of the elastic column, the large rotation behavior of plain concrete after penetration of crack and the post-peak behavior of the reinforced concrete beam including damage localization, rebar buckling and its confinement effect, which cannot be reproduced by the existing model. In the future, we will conduct further experiments including detailed measurements on post-peak behavior or collapse behavior of reinforced concrete structures and will conduct further verification and validation of the model.

REFERENCES

[1] Pijaudier-Cabot, G., Bažant, Z. P., 1987. Nonlocal Damage Theory. *Journal of Engineering Mechanics* **113(10)**:1512-1533.

[2] Peerlings, R., De Borst, R., Brekelmans, W., De Vree, J. and Spee, I., 1996. Some observations on localisation in non-local and gradient damage models. *European Journal of Mechanics-A/Solids* **15(6)**:937-953.

[3] Bažant, Z. P. and Jirásek, M., 2002. Nonlocal integral formulations of plasticity and damage: survey of progress. *Journal of Engineering Mechanics* **128(11)**:1119-1149.

[4] Bažant, Z. P., Tabbara, M. R., Kazemi, M. T. and Pijaudier-Cabot, G., 1990. Random particle model for fracture of aggregate or fiber composites. *Journal of Engineering Mechanics* **116(8)**:1686-1705.

[5] Schlangen, E. and van Mier, J.G.M., 1992. Experimental and numerical analysis of micromechanisms of fracture of cement based composites. *Cement and Concrete Composites* **14**:105-118.

[6] Jirásek, M. and Bažant, Z. P. 1995. Particle model for quasibrittle fracture and application to sea ice. *Journal of Engineering Mechanics* **121(9)**:1016-1025.

[7] Schlangen, E. and Garboczi, E.J., 1997. Fracture simulations of concrete using lattice models: Computational aspects. *Engineering Fracture Mechanics* **57**:319-332.

[8] Cusatis, G., Bažant, Z. P. and Cedolin, L., 2003. Confinement-shear lattice model for concrete damage in tension and compression: I. Theory. *Journal of Engineering Mechanics* **129(12)**:1439-1448.

[9] Cusatis, G., Bažant, Z. P. and Cedolin, L., 2003. Confinement-shear lattice model for concrete damage in tension and compression: II. Computation and validation. *Journal of Engineering Mechanics* **129(12)**:1449-1458.

[10] Kawai, T., 1978. New discrete models and their application to seismic response analysis of structures. *Nuclear Engineering and Design* **48(1)**:207-229.

[11] Bolander, J. E. and Saito, S., 1998. Fracture analysis using spring network with random geometry. *Engineering Fracture Mechanics* **61**:569-591.

[12] Nagai, K. Sato, Y. and Ueda, T., 2005. Mesoscopic Simulation of Failure of Mortar and Concrete by 3D RBSM. *Journal of Advanced Concrete Technology* **3(3)**:385-402.

[13] Yamamoto Y., Nakamura H., Kuroda I. and Furuya N., 2008. Analysis of compression failure of concrete by three-dimensional rigid body spring model. *Doboku Gakkai Ronbunshuu E* **64(4)**:612-630. [in Japanese]

[14] Yamamoto Y., Nakamura H., Kuroda I. and Furuya N., 2010. Analysis of Uniaxial Compression Failure of Confined Concrete by Three Dimensional Rigid Body Spring Model. *Doboku Gakkai Ronbunshuu E* **66(4)**:433-451. [in Japanese]

[15] Gedik Y. H., Nakamura H., Yamamoto Y., and Kunieda M., 2011. Evaluation of Three dimensional Effects in Short Deep Beams using a Rigid Body Spring Model. *Cement and Concrete Composites* **33-9**:978-991.

[16] Gedik Y. H., Nakamura H., Yamamoto Y., Ueda N. and Kunieda M., 2012. Effect of Stirrups on the Shear Failure Mechanism of Deep Beams. *Journal of Advanced Concrete Technology* **10**:14-30.

[17] Yamamoto Y., Nakamura H., Kuroda I. and Furuya N., 2014. Crack propagation analysis of reinforced concrete wall under cyclic loading using RBSM. *European Journal of Environmental and Civil Engineering, Special Issue: Control of cracking of RC structures: CEOS.fr international benchmark* **18(7)**:780-792.

[18] Mendoza. R. J., Yamamoto Y., Nakamura H. and Miura T., 2018. Numerical evaluation of localization and softening behavior of concrete confined by steel tubes. *Structural concrete* **19(6)**:1956-1970.

[19] Cornelissen, H.A.W., Hordijk, D.A. and Reinhardt, H.W., 1986. Experiments and theory for the application of fracture mechanics to normal and lightweight concrete, *fracture toughness and fracture energy of concrete* :565–575.

[20] Fujikake, K., Shinozaki, Y., Ohno, T., Mizuno, J. and Suzuki A., 1999. Post-peak and strain-softening behaviors of concrete materials in compression under rapid loading. *Proceedings of JSCE* **627(44)**:37–54. [in Japanese]

[21] Kotsovos, M. D. and Newman, J. B., 1978. Generalized stress - strain relations for concrete", *Journal of the Engineering Mechanics Division* **104(4)**:845–856.

[22] Toi, Y., 1991. Shifted Integration Technique in One-Dimensional Plastic Collapse Analysis Using Linear and Cubic Finite Elements. *International Journal for Numerical Methods in Engneering* **31**:1537-1552.

[23] Dvorkin, E. N., Onte, E. and Oliver, J., 1988. On a non-linear formulation for curved Timoshenko beam elements considering large displacement/rotation increments. *International Journal for Numerical Methods in Engineering* **26(7)**:1597-1613.

[24] Bolander, J. E., Yoshitake, K., and Thomure, J., 1999. Stress analysis using elastically uniform rigid-body-spring networks. *Journal of Structural Mechanics and Earthquake Engineering* **633(I-49)**:25-32.

[25] Timoshenko, S. and Gere, J., 1961. Theory of elastic stability, McGraw-Hill Inc.